IJC
International Journal of Cancer

In vivo characterization of brain metabolism by ^{1}H MRS, ^{13}C MRS and ^{18}FDG PET reveals significant glucose oxidation of invasively growing glioma cells

Marta Lai[1], Irene Vassallo[2], Bernard Lanz[1], Carole Poitry-Yamate[3], Marie-France Hamou[2], Cristina Cudalbu[3], Rolf Gruetter[1,3,4,5] and Monika E. Hegi[2]

[1] Laboratory for Functional and Metabolic Imaging (LIFMET), École Polytechnique Fédérale de Lausanne, Lausanne (EPFL), Switzerland
[2] Laboratory of Brain Tumor Biology and Genetics, Service of Neurosurgery and Neuroscience Research Center, Lausanne University Hospital (CHUV), Lausanne, Switzerland
[3] Center for Biomedical Imaging (CIBM), EPFL, Lausanne, Switzerland
[4] Department of Radiology, University of Geneva (UNIGE), Geneva, Switzerland
[5] Department of Radiology, University of Lausanne (UNIL), Lausanne, Switzerland

Glioblastoma are notorious for their highly invasive growth, diffusely infiltrating adjacent brain structures that precludes complete resection, and is a major obstacle for cure. To characterize this "invisible" tumor part, we designed a high resolution multimodal imaging approach assessing *in vivo* the metabolism of invasively growing glioma xenografts in the mouse brain. Animals were subjected longitudinally to magnetic resonance imaging (MRI) and ^{1}H spectroscopy (MRS) at ultra high field (14.1 Tesla) that allowed the measurement of 16 metabolic biomarkers to characterize the metabolic profiles. As expected, the neuronal functionality was progressively compromised as indicated by decreasing *N*-acetyl aspartate, glutamate and gamma-aminobutyric acid and reduced neuronal TCA cycle (−58%) and neurotransmission (−50%). The dynamic metabolic changes observed, captured differences in invasive growth that was modulated by re-expression of the tumor suppressor gene WNT inhibitory factor 1 (WIF1) in the orthotopic xenografts that attenuates invasion. At late stage mice were subjected to ^{13}C MRS with infusion of [1,6-^{13}C]glucose and ^{18}FDG positron emission tomography (PET) to quantify cell-specific metabolic fluxes involved in glucose metabolism. Most interestingly, this provided the first *in vivo* evidence for significant glucose oxidation in glioma cells. This suggests that the infiltrative front of glioma does not undergo the glycolytic switch *per se*, but that environmental triggers may induce metabolic reprograming of tumor cells.

Introduction

Glioblastoma (GBM) are difficult to treat. The functional plasticity of glioma stem-like cells, the heterogeneity within glioma cell populations, along with their high migratory potential are main obstacles toward an effective treatment. Little is known on the metabolism of the invasive tumor front. While mostly invisible to magnetic resonance imaging (MRI), it lies outside the resected and irradiated area, and is highly relevant for tumor recurrence. The latter has been further emphasized in a recent cell tracing model, demonstrating

Key words: metabolism, glioma invasion, glucose oxidation, *in vivo* magnetic resonance spectroscopy, glioblastoma

Abbreviations: Ala: alanine; CMR: cerebral metabolic rate; Cr: creatine; ^{18}FDG PET: 2-^{18}fluor-2-desoxy-D-glucose positron emission tomography; FE: fractional enrichment; GABA: gamma-aminobutyric acid; GBM: glioblastoma; Glc: glucose; Gln: glutamine; Glu: glutamate; Gly: glycine; GPC: glycerophosphocholine; GSH: glutathione; hNCL: human nucleolin; Ins: myo-inositol; Lac: lactate; Mac: macromolecules; MRI: magnetic resonance imaging; MRS: magnetic resonance spectroscopy; NAA: *N*-acetyl aspartate; PC: pyruvate carboxylase; PCA: principal component analysis; PCho: phosphocholine; PCr: phosphocreatine; SD: standard deviation; SNR: signal to noise ratio; SUV: standardized uptake values; Tau: taurine; TCA cycle: tricarboxylic acid cycle; tCho: total choline; VOI: volume of interest; WIF1: WNT inhibitory factor 1

Additional Supporting Information may be found in the online version of this article.

Conflict of interest: The authors declare no conflict of interest concerning this study.

Grant sponsor: Leenaards and Jeantet Foundations; **Grant sponsor:** European Union's Seventh Framework Programme; **Grant number:** FP7-PEOPLE-2010-ITN-264780; **Grant sponsor:** Swiss National Science Foundation; **Grant number:** 31003A-138116

DOI: 10.1002/ijc.31299

History: Received 30 Oct 2017; Accepted 31 Jan 2018; Online 8 Feb 2018

Correspondence to: Monika E. Hegi, Department of Clinical Neurosciences, CHUV, Chemin des Boveresses 155, Epalinges CLE-C306, Switzerland, Tel.: 41-21-314-25-82, E-mail: monika.hegi@chuv.ch; or Cristina Cudalbu, CIBM, EPFL, Lausanne, Switzerland, E-mail: cristina.cudalbu@epfl.ch

What's new?

Glioblastomas are diffusely infiltrative tumors with an invasive margin that frequently lies beyond resected and irradiated areas of the brain. It is suspected that invasive glioma cells sustain diffusely infiltrative growth in microenvironments with an intact blood barrier via unique metabolic modifications. Here, using ^{1}H-Magnetic resonance spectroscopy (MRS) at ultra-high magnetic field, 16 metabolites were monitored during invasive growth of patient-derived glioblastoma xenografts in the mouse brain. *In vivo* cell-specific flux analysis by ^{18}FDG-PET and ^{13}C-MRS revealed significant glucose oxidation of invasively growing glioma cells, challenging the Warburg effect, according to which cancer cells rely primarily on glycolytic metabolism.

a large overlap between cell clones in the invading front and tumor sustaining clones after serial orthotopic transplantation of human GBM cells in mice.[1] Invading cells usually grow at low cell density, surviving in a specific micro-environment with an intact blood–brain barrier and availability of oxygen and nutrients, suggesting that these tumor cells require distinct treatments. The characterization of the metabolic modifications associated with the invasive phenotype may help to target metabolic pathways relevant for invading cells.

The determination of the altered metabolic profiles in GBM can be achieved *in vivo* in xenograft models using ^{1}H, ^{13}C magnetic resonance spectroscopy (MRS) and ^{18}FDG positron emission tomography (^{18}FDG PET).[2,3] The determination of neurochemical profiles with ^{1}H MRS *in vivo* at ultrahigh magnetic field (i.e., 14.1 T) using short echo-time sequences allows the simultaneous detection of a large number of metabolites that otherwise display highly superimposed signals, such as glutamate and glutamine, phosphocholine and glycerophosphocholine, creatine and phosphocreatine, myo-inositol and glycine.[4,5] The metabolites that become detectable provide insights into energy metabolism, myelination, neurotransmission, antioxidation and osmoregulation, as recently reported from rodent xenograft models of glioma.[6,7]

The combination of ^{18}FDG PET and ^{13}C MRS *in vivo* allows the assessment of glucose metabolism through aerobic and anaerobic pathways. While PET measures total glucose consumption without distinguishing between different metabolic pathways subsequent to glucose phosphorylation, ^{13}C MRS assesses during the infusion of ^{13}C-labeled glucose the incorporation of the stable isotope ^{13}C into metabolites downstream of glycolysis, such as glutamate and glutamine. This aspect is of particular interest in the current debate on cancer metabolism and mitochondria as recent *ex vivo* studies have provided for the first time evidence for active glucose oxidation in human GBM cells,[8,9] while standard teaching on tumor cell metabolism decrees that tumor cells would preferentially metabolize glucose to lactate, the so-called Warburg effect.

Therefore, the overall aim of the present longitudinal study was to identify the temporal metabolic modifications in a highly infiltrating and non-necrotic mouse glioma xenograft model, whose invasive properties and outcome were modulated by expression of the tumor suppressor gene WNT inhibitory factor 1 (*WIF1*).[10] The use of an *in vivo* multimodal imaging approach with ^{1}H MRS and MRI at ultrahigh magnetic field (14.1 T) and short echo-time allowed longitudinal measures of 16 brain metabolites to characterize tumor infiltration. Late stage metabolism was examined with ^{18}FDG PET and ^{13}C MRS upon infusion of [1,6-^{13}C]glucose, and subjected to compartmentalized metabolic flux analysis to elucidate metabolic fates of glucose in GBM cells.

Methods

Orthotopic mouse glioma model

GBM sphere cells LN-2669GS (10^5 cells) transduced with either the WIF1 expression vector (LN-2669GS_*WIF1*) or the empty vector control (LN-2669GS_*pIRES2*) were stereotaxically injected into the caudoputamen of male Swiss nu/nu mice as previously described.[10] The use of male mice avoids potential effects of the oestrous cycle on the metabolism. The parental GBM sphere line LN-2669GS has been established and maintained in our laboratory under stem cell conditions as described previously,[11] and has been molecularly characterized (*TP53* wild-type, *PTEN* mutant, *NF1* mutant, *CDKN2A* homozygous deletion; GEO accession numbers GSE60274, GSE108098 and GSE104291 for DNA methylation, aCGH and gene expression data, respectively), and authenticated by DNA fingerprinting.[11–13] The mice entered into our study correspond to a subset of a larger cohort (15/20) demonstrating a tumor suppressing effect of *WIF1* as reported previously.[10] Experimental and molecular description of the model *in vitro* and *in vivo* is available in Vassallo *et al.*[10] Mice exhibiting tumor growth between the dura and the skull were excluded (3/15) to avoid potential artifacts, as the tumor mass compresses the underlying brain leading to gliosis. All animal experiments were approved by the veterinary authorities (VD1181.3-6).

In vivo ^{1}H magnetic resonance spectroscopy

All MRI/MRS experiments were carried out in a 14.1 Tesla 28-cm horizontal bore animal scanner (Agilent Technologies, Palo Alto, CA). *In vivo* ^{1}H MRS was performed with a short echo-time (TE = 2.8 ms) spin echo full-intensity sequence.[4] Quantitative ^{1}H MRS data were obtained as absolute concentrations (in micromole/g) using water as internal reference.[3,14] The experimental and technical details are described in the Supporting Information methods.

In vivo ^{18}FDG positron emission tomography

Injected mice were scanned with ^{18}FDG PET at presentation of first neurological symptoms, and left to recover for 24–36 hr before the ^{13}C labeling experiment. Age-matched control mice were scanned under identical conditions. All experimental procedures were carried out with an avalanche photodiode micro-PET scanner (LabPET4, Gamma Medica, Sherbrooke, Canada). A bolus of ^{18}FDG was administered through the tail catheter during the first 10 sec of the scan (1.4 ± 0.2 MBq/g; mean $\pm$ SD), followed by a saline chase (100–150 μL). The total duration of the scan was 50 min to reach a steady-state in ^{18}FDG kinetics to determine the FDG standardized uptake value. See Supporting Information methods for details.

In vivo ^{13}C magnetic resonance spectroscopy and metabolic flux analysis

In brief, mice were fasted for 7 hr with free access to water before experiments, to deplete endogenous glucose. *In vivo* ^{1}H MRS was performed on the volume of interest (112 μL, 3.7 mm × 6.9 mm × 4.5 mm covering the striatum in both hemispheres, or 60 μL, 3.6 mm × 3.7 mm × 4.5 mm) to quantify the neurochemical profile in the region and to quantify glutamate (Glu) and glutamine (Gln) pool size. Total metabolite concentrations are assumed to remain constant throughout the scan. Glycemia was measured before labeled glucose injection. A 5 min bolus injection was followed by 4 hr of continuous infusion of [1,6-^{13}C]glucose to reach steady-state labeling conditions in plasma glucose (70% fractional enrichment). The acquired dynamic ^{13}C MRS spectra were scaled to absolute concentrations using the ^{13}C multiplet patterns of the glutamate resonances and the total glutamate pool size, enabling a fully quantitative determination of the metabolic fluxes. The standardized infusion protocol and the detection techniques are detailed in the Supporting Information methods.

Individual time courses of ^{13}C labeling for glutamate and glutamine C4, C3 and C2 were integrated into a modified two-compartment model for brain metabolism in which one compartment is assigned to neurons, while the other is shared between glial and GBM cells, based on the hypothesis that the glucose metabolism in GBM cells is structurally similar to glial cells. This model assumes that GBM cells actively oxidize glucose and acetate, as previously shown in *ex vivo* models.[8,15] Glutamine is mainly oxidized from glucose and catabolism of blood-born glutamine is not found to be significant in such cells.[8] A more detailed description of the model assumptions and differential equations is described elsewhere[16] and Supporting Information methods.

Quantification of human glioma and mouse cells

Coronal brain sections in the plane of the injection were immunostained for human nucleolin (hNCL) as described, to identify the human glioma cells.[10] Human glioma cells and mouse cells were quantified in a square of 0.5 mm^2, placed at the location evaluated for metabolite concentrations by ^{1}H MRS (Fig. 1).

Statistical analyses

The concentrations of the metabolites were examined by principal component analysis (PCA). A Monte-Carlo Test (999 permutations; global test) was performed to test overall difference between groups.[17] The missing values were imputed by regularized iterative PCA algorithm.[18] All analyses and graphical representations were performed in R (URL http://www.R-project.org) and the R packages missMDA and ade4.[19,20] Statistical significance of metabolite concentrations between groups and between maximum/minimum values at each time point and initial values were evaluated with Student's *t*-test. Linear correlations were tested by determining R^2, the slope and the *p*-values for the null hypothesis (zero slope of the regression line) for each group. *p*-Values ≤ 0.05 were considered statistically significant.

Results

To assess the temporal changes of metabolic profiles capturing the evolution of tumor growth, *in vivo* ^{1}H MR images and spectra were acquired longitudinally at 14.1 Tesla of a highly invasive orthotopic glioma model (Fig. 1). Tumor bearing mice followed and analyzed in our study were part of a larger cohort (12/20) of a project investigating the mechanistic effects of re-expression of the tumor suppressor gene *WIF1* on invasion and migration *in vivo* and *in vitro* as reported previously.[10] First scans were performed 6 weeks after injection of the mice and repeated every week, as illustrated for all mice in Supporting Information Figure S1 ($n = 8$, injected with the GBM-derived sphere-line LN-2669GS_WIF1; $n = 4$, injected with vector control LN-2669GS_pIRES2; $n = 7$, non-injected age-matched control mice). T_2-weighted images were devoid of focal tumors, and tumor progression was not visible on MR images. However, the injected side of the striatum appeared expanded, influencing the ventricle size (Fig. 1*a*). At final sacrifice, visualization of the human cells by immunohistochemistry revealed diffuse distribution of the glioma cells in both hemispheres (Fig. 1*b*) with a human/mouse cell ratio between 0.3 and 1.8. However, there was one exception: in mouse NCH-1444 the tumor was visible on MRI and human cells were mainly restricted to the injected side with a higher cell density (ratio human/mouse 2.6), and exhibiting a diffuse growth pattern (Fig. 1*b*). Due to the distinct behavior, NCH-1444 was treated separately in the following analyses (green in the graphics).

^{1}H MRS at ultrahigh magnetic field (14.1 Tesla) and short echo time provided excellent sensitivity (SNR = 16–27 in 8 μL) and spectral resolution allowing quantification of 16 distinct metabolites simultaneously, such as glycine (Gly) and myo-inositol (Ins), creatine (Cr) and phosphocreatine (PCr), glycerophosphocholine (GPC) and phosphocholine (PCho)

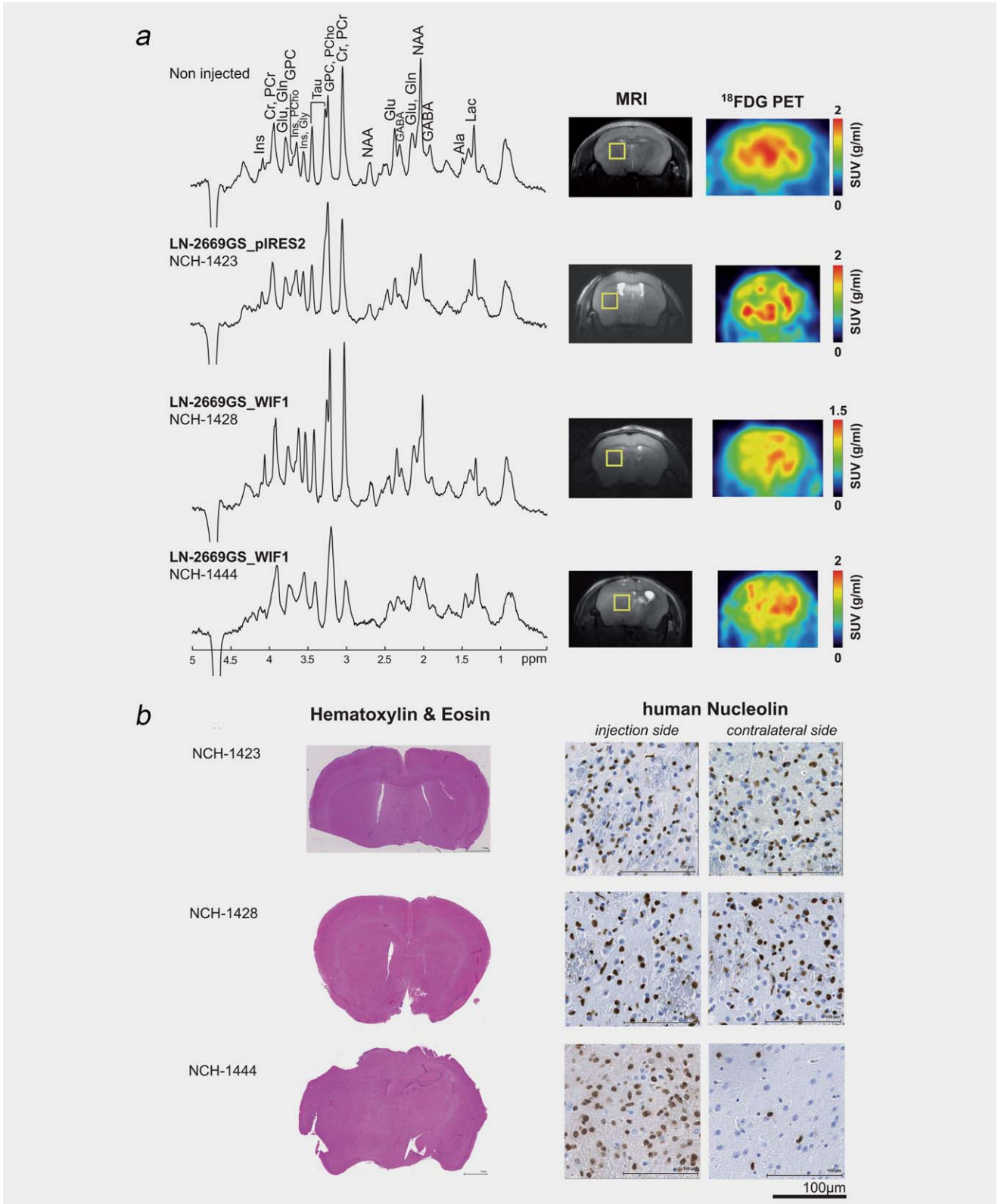

Figure 1. ^{1}H Magnetic resonance spectroscopy and PET of orthotopic glioma xenografts. (*a*) ^{1}H MRS spectra obtained at 14.1 Tesla from a localized volume of 2 mm × 2 mm × 2 mm in the right striatum of a non-injected mouse, a mouse injected with LN-2669GS_pIRES2 cells (14 weeks after injection, NCH-1423) and two mice injected with LN-2669GS_WIF1 cells (NCH-1428, 17 weeks; NCH-1444, 16 weeks). Corresponding axial slices of T2-weighted images and ^{18}FDG PET are shown on the right (SUV, standard uptake values). In NCH-1444 the tumor was mostly confined to the injected side. The MRI images correspond to the images shown in Figure 5, since they were taken before ^{1}H and ^{13}C MRS during the same scanning session for each animal. (*b*) The respective tumor-bearing mouse brains (NCH-1423, NCH-1428) are shown, stained for hematoxylin and eosin (H&E), and anti-human Nucleolin (hNCL) that detects human cells visualizing the highly invasive properties in the injected and the contra-lateral side. NCH-1444 is an exception in the series. The distribution of the human tumor cells indicates an invasive tumor that is basically confined to the injected side (human/mouse cells = 2.6) compared to only few tumor cells on the contralateral side. [Color figure can be viewed at wileyonlinelibrary.com]

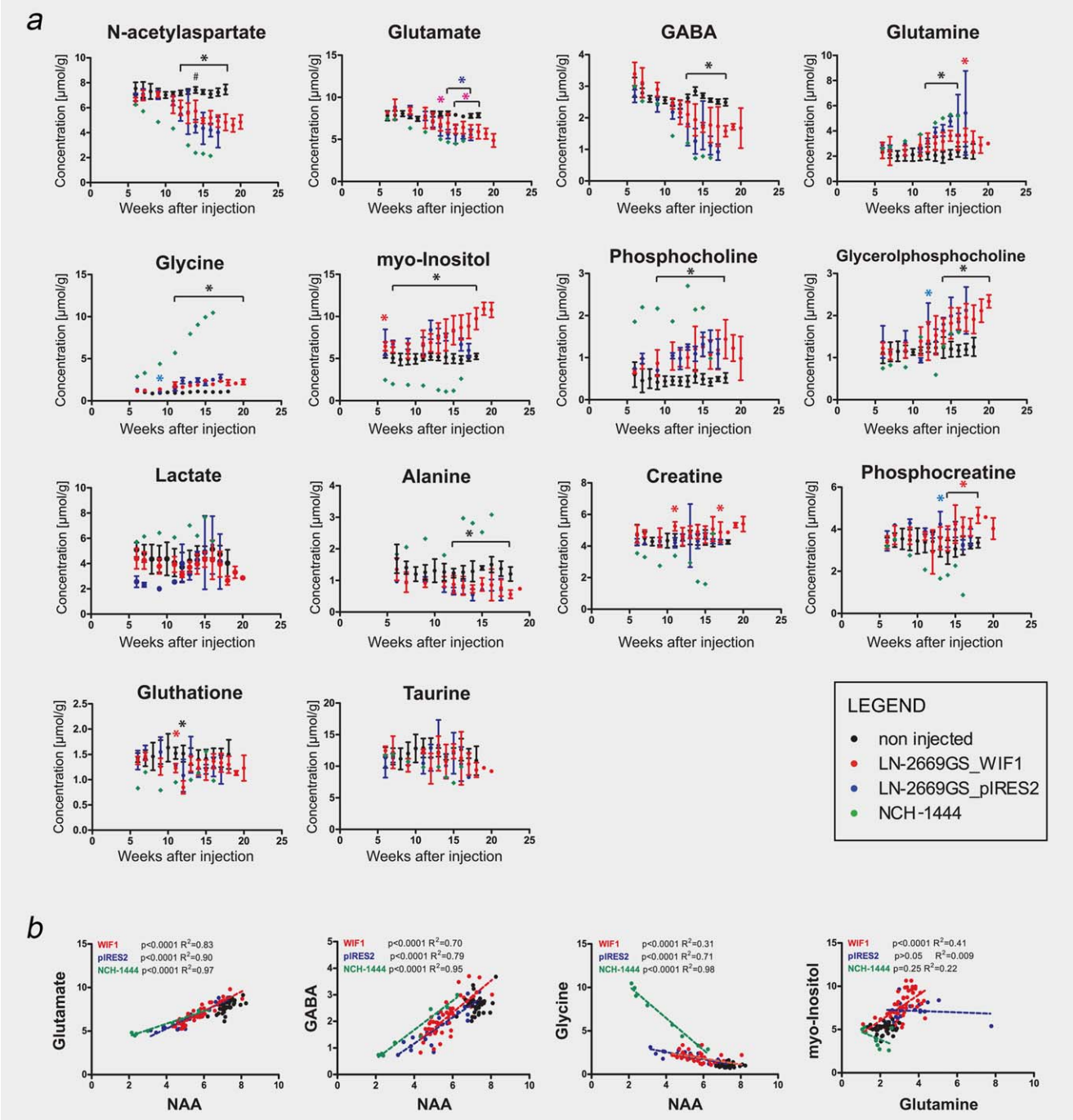

Figure 2. ^{1}H MRS data acquired during tumor development. (*a*) Longitudinal measurements of brain metabolites between Week 6 and Week 17 post injection. Non-injected mice (black), mice injected with LN-2669GS_pIRES2 (blue) and LN-2669GS_WIF1 (red), respectively. Mouse NCH-1444 (LN-2669GS_WIF1) is an outlier, shown separately in green. Results are presented as averages ± SD (µmol/g). Black asterisks indicate a significant difference ($p < 0.05$) for both groups while blue or red asterisks show significant differences for the pIRES2 and WIF1 group, respectively. (*b*) Correlations between the concentration of NAA, a highly specific neuronal marker, and the neurotransmitters glutamate, GABA and glycine. Points represent measured concentrations in a single mouse at a single time point expressed in µmol/g. The linear fit curve and the respective statistics are shown for the pIRES2 and WIF1 group, and for NCH-1444, separately.

(Figs. 1 and 2). Metabolite concentrations and profiles determined longitudinally in non-injected mice were similar to previous studies.[21] The temporal evolution of the metabolite concentrations averaged for each group at every time point is reported in Figure 2*a*. The first signs of tumor development appeared at Week 7 after injection and manifested as a statistically significant increase in PCho and Ins, followed by a reduction in *N*-acetyl aspartate (NAA) (Fig. 2*a*). Gly

increased after Week 11. NAA decreased steadily, reaching a plateau for long-term surviving mice (~5 μmol/g at 18–20 weeks). The same fate was shared by the main neurotransmitters Glu and GABA. PCho reached a maximum increase between 16 and 18 weeks and tapered off thereafter. In contrast, GPC, and Gly showed a significant linear increase and alanine (Ala) a significant decrease until final sacrifice. All other metabolites only showed increased variability over time, without a clear evolution pattern. NCH-1444 behaved as an outlier that may reflect the distinct growth pattern. Significant positive linear correlations were observed between concentrations of NAA and the neurotransmitters Glu, and gamma-aminobutyric acid (GABA), and a significant negative correlation with Gly (Fig. 2*b*).

The metabolic profiles obtained by MRS for all mice over time were analyzed by PCA (Fig. 3*a*). The main structure of the data was explained by the first axis (40.5% of inertia) mostly characterized by metabolites linked to neuronal metabolism (NAA, Glu and GABA) that are negatively correlated with markers specific for high cellular turnover such as choline compounds. Gly, Gln and Ins resulted in relevant projection on the same axis, although shorter than NAA, Glu and GABA. No difference was observed between the two different tumor groups (WIF1 *vs.* empty vector; p-values = 0.09) when time was not considered (Fig. 3*a*). The non-injected mice (projected, but not active in the PCA) were homogeneous, characterized by elevated concentration of NAA, Glu and GABA.

A gradual change of the PCA values was observed over time associated with diffuse tumor growth (Fig. 3*b*) as reflected by modified metabolic profiles measured by the means of ^{1}H MRS (Figs. 1*a* and 2*a*). At early time points, both the controls and the injected mice are located in the same region defined by neuron-related metabolites. Injected mice shifted over time to the region characterized by metabolite markers for high cell turnover (choline compounds), while the metabolite profiles of the non-injected mice did not change (Fig. 3*b*). The lowess curve for WIF1 expressing xenografts is shifted towards later time points as compared to the vector control, although it did not reach significance. The trend toward later time points is in agreement with a tumor suppressing effect of WIF1 that prolongs survival of the mice as determined in the complete mouse cohort (see Methods)[10] and other orthotopic glioma xenograft models.[10,22] NCH-1444 showed a more pronounced evolution over time, in line with the distinct metabolic features described above (Figs. 2*a* and 2*b*).

Last time point analysis: association between metabolites and tumor burden

When tumor bearing mice presented first neurologic symptoms a last ^{1}H MRS scan was performed before sacrifice. The metabolic profiles linked to the symptomatic tumor-stage typically featured significantly increased concentrations of total choline (tCho, GPC + PCho), lower NAA, Glu and GABA, and higher Gln and Ins (Figs. 1*a* and 2*a*). Of note, no elevated lactate levels were observed. Similar to the longitudinal analysis, the first axes of the PCA (39.6% of inertia) of the end stage profiles was dominated by NAA, GABA and Glu, in anti-correlation with tCho (Fig. 4*a*). PCho projection on the first axis is close to zero, while GPC is mostly aligned with tCho (Fig. 4*a*), reflecting a more important contribution of GPC to tCho increase at late stage compared to PCho. Taurine (Tau) and macromolecules (Mac) have a long projection on the same axis strongly correlated with NAA. The second axis (20% of inertia) is related to Ala, lactate (Lac), Gln and Ins. The tumor density was classified into LOW and HIGH (ratio human/mouse cells ≤ 1 *vs.* >1), visualized by the ellipses in Figure 4*a*. The difference between the groups did not reach significance on the first axis of the PCA (p-values = 0.18, Fig. 4*b*). However, using continuous values, the coordinates of the mice on the first axis were significantly correlated with their tumor cell ratio (Fig. 4*c*, Spearman correlation, $r = 0.682$, p-values = 0.025). HIGH density tumors were characterized by markers of membrane turnover (choline compounds), while the LOW density tumors were associated with healthy neuronal metabolism (NAA, Glu, GABA and Tau).

Significant linear relationships between individual metabolites and the ratio human/mouse cells were found for NAA, Glu, Gly, GPC and Mac (Fig. 4*d*), but not PCho, Ins and Gln, that were, however, measured at higher concentrations compared to non-injected mice. The remaining metabolites were uncorrelated with the increasing relative number of glioma cells. Of note, no difference was found between the mice injected with WIF1 cells or the vector control at the time of sacrifice (Supporting Information Fig. S2). This was in agreement with the overall analyses when ignoring time (Fig. 2*a*) and was expected given that all mice were symptomatic at the time of sacrifice.

To assess glucose metabolism ^{18}FDG PET acquisitions were performed after the last ^{1}H MRS scan, which did not show increased standardized uptake values (SUV) for glucose in the volume of interest examined during ^{1}H MRS scans ($SUV_{inject} = 1.4 \pm 0.4$ g/mL; 8 μL, right striatum) compared to the contralateral side ($SUV_{contra} = 1.3 \pm 0.2$ g/mL, left striatum). Comparable SUV values were found in the left striatum of non-injected mice (1.7 ± 0.3 g/mL). Therefore, glucose uptake was not found to increase locally in presence of GBM cells at late stage (Fig. 1*a*).

Brain energy metabolism was measured by ^{13}C MRS in 6 glioma-bearing mice by infusing [1,6-^{13}C]glucose as a last experiment. For subsequent metabolic flux analysis, fractional enrichment (FE) curves were averaged over 3 mice with similar metabolite profiles and human/mouse cell ratio (1.7–1.8, Fig. 4; Supporting Information Figs. S3 and S4). Spectra from NCH-1444 are shown separately in Figure 5*c* as an extreme case of a cell dense tumor environment (human/mouse cell ratio = 2.6). ^{13}C MRS spectra were acquired *in vivo* over 4 hr. Results collected in glioma bearing mice were compared to data from similar labeling experiments performed on 6 non-injected mice.[16] The glutamate pool was significantly

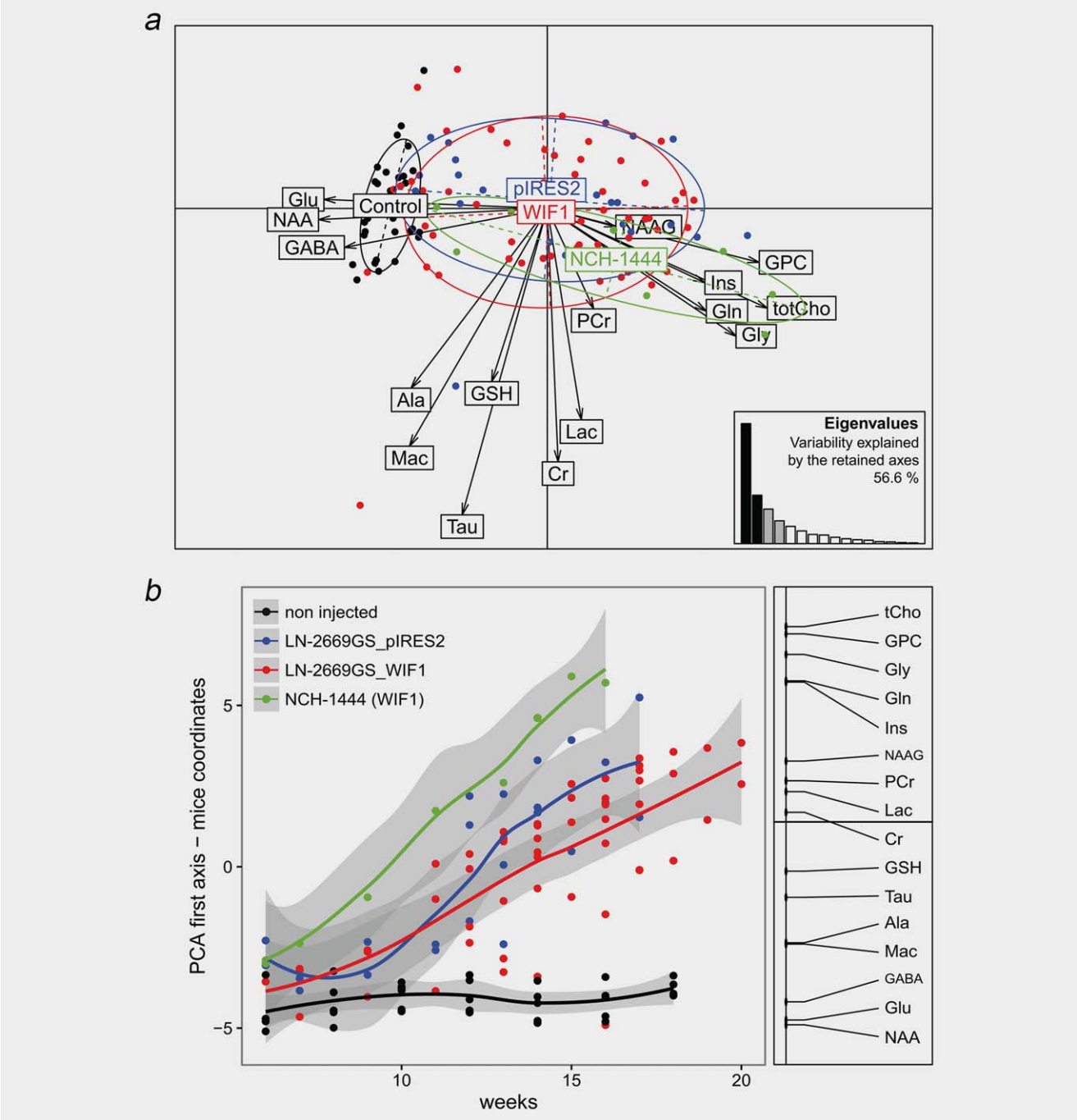

Figure 3. Longitudinal metabolite profiles. (*a*) Biplot of the PCA of the longitudinal metabolite profiles. Each scan is indicated by a dot (black, control, non-injected mice; red, mice injected with LN-2669GS_WIF1 cells; blue, mice injected with LN-2669GS_pIRES2 cells; green, NCH-1444). The inertia ellipses visualize the mice corresponding to the three groups. The non-injected mice and NCH-1444 are visualized, but not active in the analysis. (*b*) Scatter plot of the mouse coordinates on the first axis plotted against time from injection (weeks). A non-parametric regression line (lowess) is added for each group to show the tendencies over time. The corresponding one-dimensional representation of the metabolite coordinates for the first axis of the PCA is shown on the right. GSH, glutathione; Mac, macromolecules.

reduced in the tumor bearing group ($p < 0.0001$), while glutamine appeared more concentrated compared to non-injected mice ($p < 0.05$) (Supporting Information Fig. S3).

In vivo spectra exhibited fully resolved resonances for the C4, C3 and C2 of Glu and Gln (Figs. 5*a* and 5*b*). Moreover, spectra acquired from only 60 μL VOI in 64 min at steady-state still featured a very good SNR (∼6) and spectral resolution (∼25 Hz) (Fig. 5*c*). Comparison between steady-state spectra acquired for 64 min after 3 hr of infusion showed a distinct labeling pattern in glioma bearing brains (Figs. 5*b*

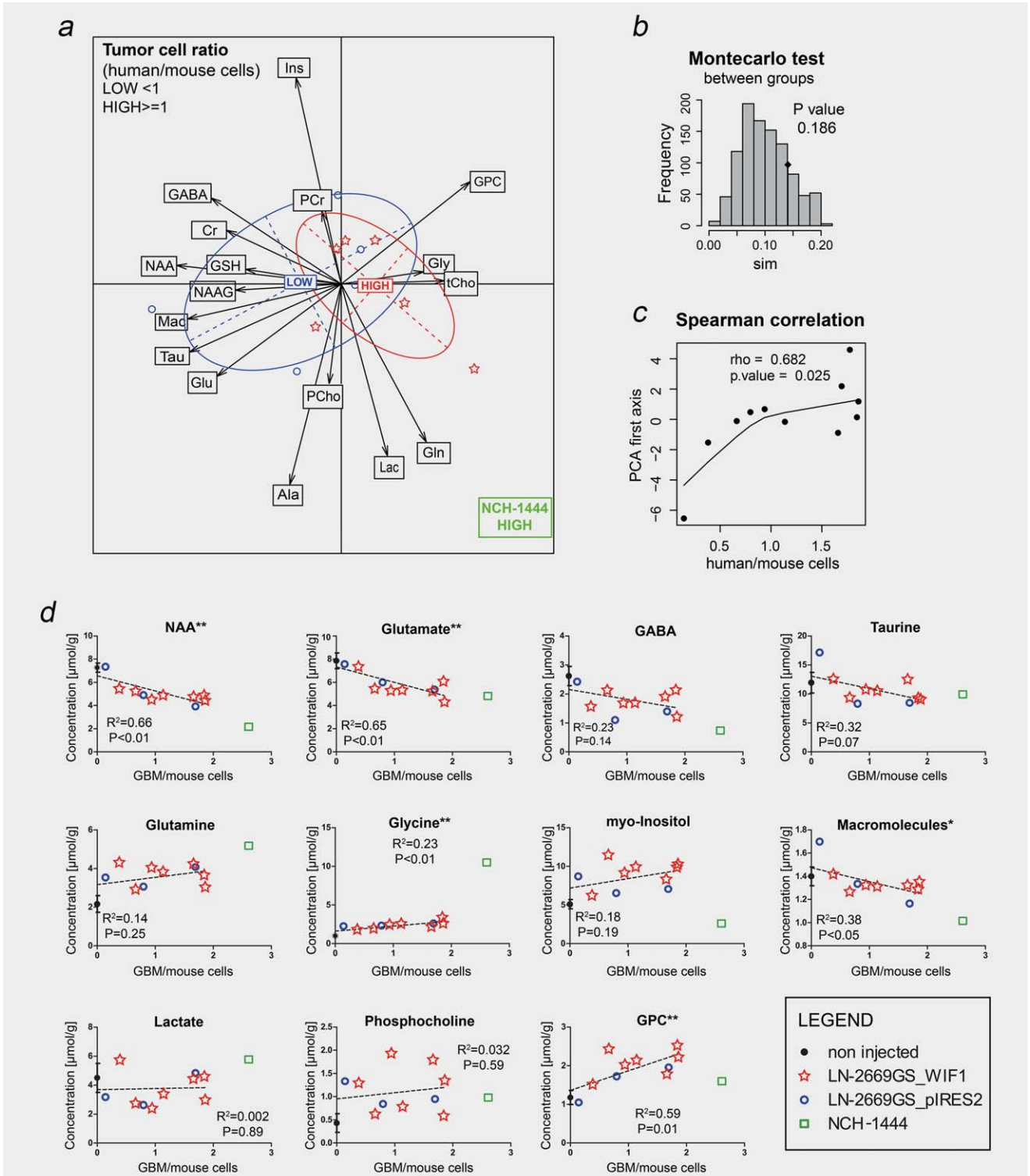

Figure 4. Metabolite profiles at the last time point and tumor cell ratio. (*a*) The metabolite profiles of all xenografts at the last time point are presented in a PCA showing the two first axes. (*b*) The ratio of tumor over host cells was used to classify the mice into HIGH and LOW, using 1 as threshold, visualized by red stars and blue circles, and corresponding inertia ellipse (p-values = 0.186); NCH-1444 (green square) is inactive in the analysis. (*c*) The correlation between the 1st axes of the metabolite profile and the density of the tumor cells (ratio human/mouse cells) is significant (rho= 0.682, p-values = 0.025). (*d*) Linear regressions established between brain metabolite concentrations at the last scan and the human/mouse cell ratio (only metabolites with significant correlation). Symbols represent single mouse measurements (µmol/g). The experimental point shown as "null content" for GBM cells represents the average metabolite concentration in non-injected mice of the same brain region (group mean ± SD). The outlier NCH-1444 (green square) is not included in the linear regression. Significant correlations are indicated (*$p < 0.05$, **$p < 0.01$, Student's t-test). [Color figure can be viewed at wileyonlinelibrary.com]

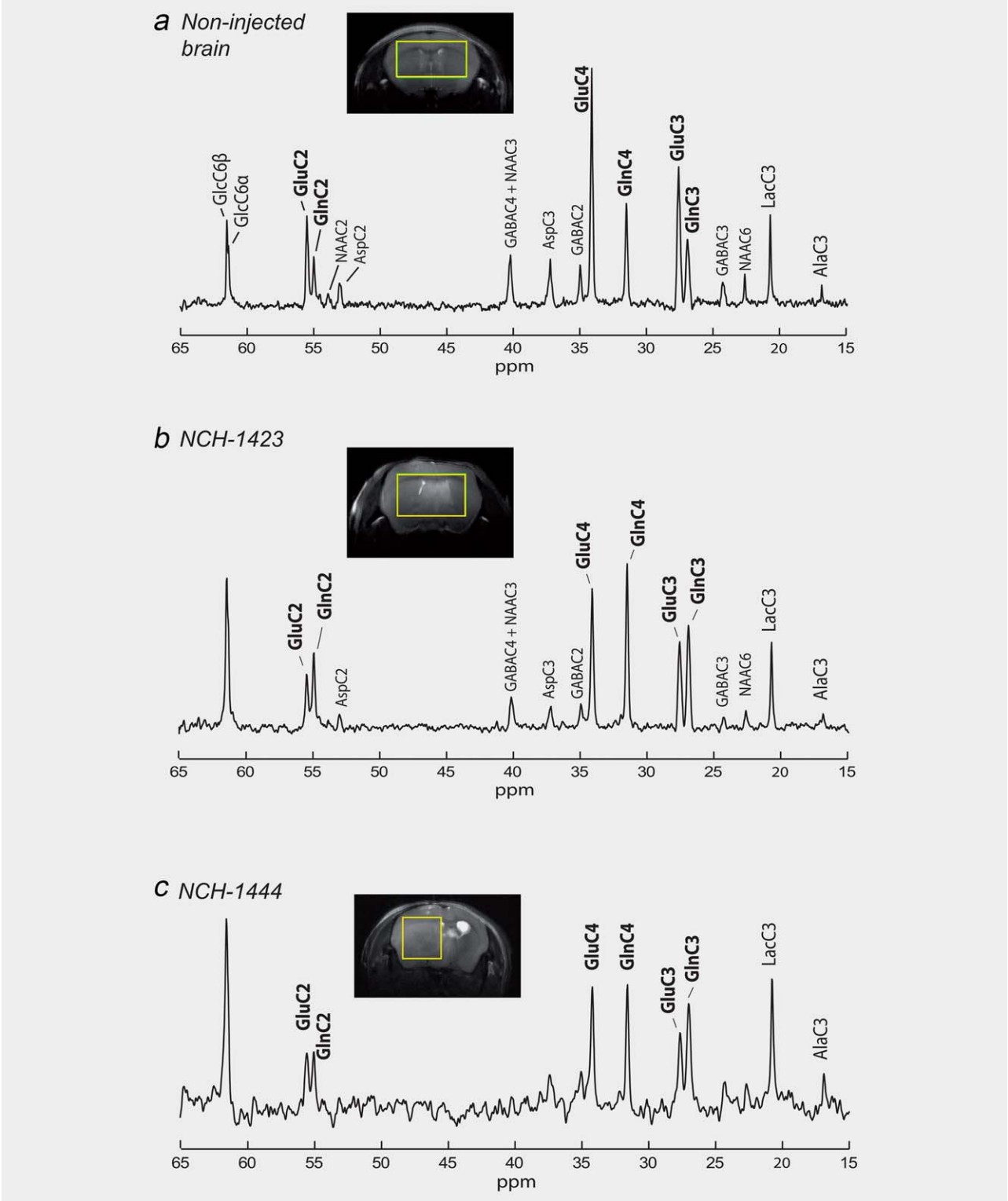

Figure 5. *In vivo* ^{13}C MR spectra acquired at steady-state of [1,6-^{13}C]glucose infusion of a control and tumor bearing brains. ^{13}C MR spectra were acquired after 3 hr of [1,6-^{13}C]glucose infusion during 64 min. The volume was 112 μL (3.6 mm × 6.9 mm × 4.5 mm) covering the central brain on both hemispheres for the non-injected mouse brain (*a*) and the brain with the invasively growing tumor NCH-1423 (*b*). NCH-1444, acquired in a 60 μL voxel (3.6 mm × 3.7 mm × 4.5mm) centered in the injected side (*c*). MRI images are the same as shown in Figure 1*a*, since they were taken before ^{1} H and ^{13}C MRS during the same scanning session for each animal. [Color figure can be viewed at wileyonlinelibrary.com]

and 5*c*) as compared to non-injected brains (Fig. 5*a*). Accumulation of labeling in Glu was reduced in all three carbon positions, while the absolute concentration in Gln-labeled carbons appeared higher as compared to control mice (Fig. 5*a*). Labeling of LacC3 from glycolysis did not appear increased in the tumor bearing brains (Figs. 5*b* and 5*c*).

Distinct time courses of Glu and Gln C4, C3 and C2 (Supporting Information Fig. S4) were fitted to a two-compartmental model for energy metabolism adapted for glioma-bearing mice (Fig. 6*a*), yielding a rate of the neuronal TCA cycle ($V^n_{TCA} = 0.22 \pm 0.02$ μmol/g/min) and the TCA cycle rate accounting simultaneously for glial and glioma cells ($V_g = 0.30 \pm 0.06$ μmol/g/min), pyruvate carboxylase activity in the glial-GBM compartment ($V_{PC} = 0.059 \pm 0.007$ μmol/g/min), and the neurotransmission rate ($V_{NT} = 0.05 \pm 0.02$ μmol/g/min). The glial-GBM compartment showed significant glucose oxidation through TCA cycle (V_g) and anaplerosis (V_{PC}), while the estimated values of neuronal TCA cycle (V^n_{TCA}) and neurotransmission (V_{NT}) were significantly lower in glioma bearing mice ($p < 0.5$ and 0.001 respectively) compared to healthy animals (respectively −58% and −50%) as visualized in Figure 6*b* (Supporting Information Table S1).

Discussion

Our study characterizes for the first time *in vivo* longitudinal metabolite profiles of an orthotopic glioma sphere line model with highly infiltrative behavior, thereby providing information on the metabolic changes during invasive growth in absence of tumor necrosis. The metabolite profiles allowed the association between tumor burden and the modification of metabolite concentrations. Moreover, compartmentalized modeling of dynamic ^{13}C MRS data allowed the distinction of neuronal metabolism from metabolism of glial and glioma cells. Using novel technology, we investigated the metabolic fates of glucose in GBM cells that have not been determined *in vivo* before. At present, our *in vivo* analysis is limited to one invasive orthotopic glioma model and further studies on other invasive models are warranted.

Infiltrating glioma cells preserve mitochondrial glucose oxidation similarly to glial cells

GBM is known for the elevated rates of glucose consumption in the regions close to the tumor core. This phenomenon, often observed in patients with ^{18}FDG PET, is thought to reflect the Warburg effect in tumor cells that promotes anaerobic glucose metabolism and Lac production, simultaneously decreasing the mitochondrial functionality. Lac concentration can be detected non-invasively by ^{1}H MRS, however, correlations with ^{18}FDG measurements in humans indicated that the Lac signal intensity is not always associated with hypermetabolic regions,[23] but may be increased in necrosis possibly due to reduced clearance.[24] Therefore, increased glucose uptake would only be effectively detected by ^{18}FDG PET. In our model, SUV maps reflecting ^{18}FDG uptake in injected mice did not show substantially increased values compared to cerebral metabolism. On the contrary, extended hypointense areas were observed by visual inspection (Fig. 1*a*), possibly reflecting a reduced glucose uptake in "suffering" cells. This apparent contradiction with the classical model of glioma metabolism is probably explained by the absence of a central necrosis in the current model used. A shift toward anaerobic metabolism is in fact typical of tumor cells in hypoxic and nutrient-restricted conditions[25] and has been recently associated with increased migration in GBM and normal brain cells,[26] with hypoxia representing the trigger for migration. In contrast, glioma cells infiltrating the normal brain have access to normal nutrient concentrations and oxygen tension and, therefore, may not require extensive metabolic reprograming to support tumor development, in agreement with the proposition that upregulation of glycolysis maybe associated with the angiogenic switch.[27] This would be compatible (i) with the relatively low levels of Lac observed in our invasive model that were comparable to non-tumor bearing mice (Figs. 1*b* and 2*a*), (ii) a minor role of Lac in the PCA during tumor evolution and at late time points (Figs. 2*a* and 3*a*) and (iii) the lack of a correlation of Lac with the ratio human/mouse cells (Fig. 4*d*). Consequently, brain tumors not affected by the Warburg effect would not be detected by PET in patients, both due to low cell density and superposition with hypermetabolic cells. It is of note, increased Lac concentrations are detected in other orthotopic glioma xenograft mouse models yielding compact tumors, and are more prominent when displaying gadolinium uptake and necrosis – indicating presence of hypoxia – as we reported previously.[7]

The absence of a necrotic core is commonly observed in xenograft models derived from glioma stem-like cells.[1,28] Necrotic regions are often associated with reduced concentrations of Glu and Gln due to neuronal loss and reduced glucose oxidation. However, the direct assessment of Glu and Gln concentration *in vivo* is quite challenging. Although their separate estimation in humans is feasible at $\geq$3 T[3], this might be further complicated by the spectral superposition with macromolecules, lipid signals in high grade gliomas and increased tissue inhomogeneity. Under these conditions, the viable tumor cells and the invasive front are even more difficult to assess with *in vivo* ^{13}C MRS due to reduced sensitivity and spatial resolution. This has limited *in vivo* ^{13}C MRS studies for the detection and modeling of Lac turnover, the most prominent signal in glycolytic tumors, such as C6 glioma bearing rats.[29] In contrast, LN-2669GS cells yield a glioma model that affects large portions of the mouse brain homogeneously, enabling for the first time the detection of ^{13}C MR spectra *in vivo* during glioma invasion. ^{13}C detection at 14.1 T allowed the accurate measurement of cell-specific metabolic fluxes *in vivo* in volumes as small as 60 μL, with the separate detection of C4, C3, C2 resonances of Glu and Gln labeled by [1,6-^{13}C]glucose (Fig. 5).

The Glu pool determined by MRS was ascribed to neurons according to the modeling scheme, as further supported by the high correlation over time of Glu with NAA, a known neuronal marker (Fig. 2*b*). Since glioma cells represented a

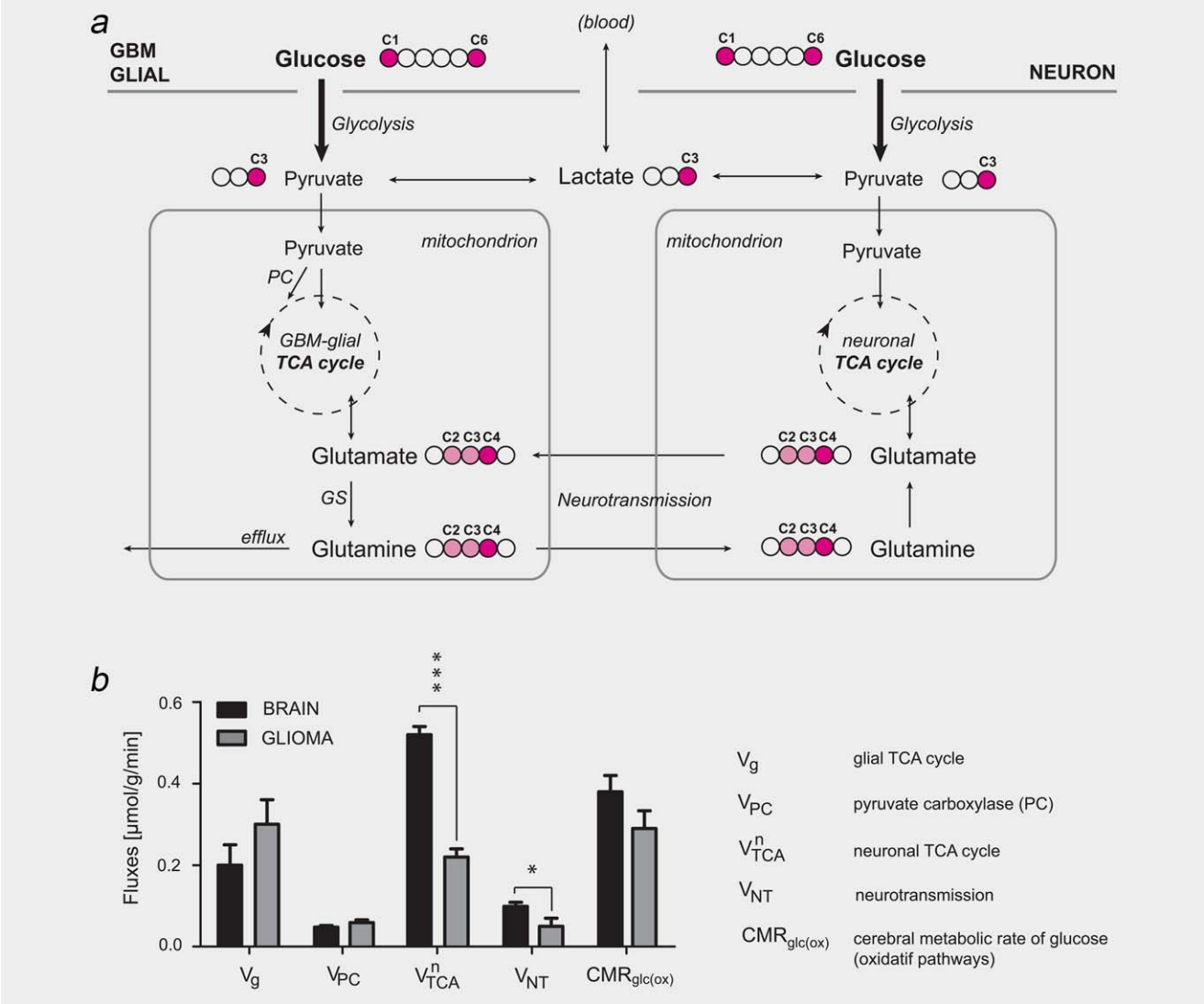

Figure 6. Metabolic modeling of *in vivo* ^{13}C MRS in glioma bearing mice. (*a*) Two-compartmental model of glucose metabolism in the brain of glioma bearing mice. Glioma cells are assumed to constitute a homogeneous pool with glial cells. The carbon skeleton of labeled molecules is shown and the labeled carbon position is colored (pink) and indicated as C_i ($i = 1,2, \ldots,6$). [1,6-^{13}C]glucose is assumed to enter brain cells (neurons, glia and glioma) and undergo glycolysis leading to labeling of [3–^{13}C]pyruvate and [3–^{13}C]lactate. The lactate pool, common to both compartments, contributes to non-oxidative pathways and is diluted from blood-born unlabeled lactate. [3–^{13}C]Pyruvate enters the mitochondria and leads to labeling of [4–^{13}C]glutamate in both compartments from the first turn of the TCA cycle (dark pink). Pyruvate carboxylase (PC) activity is considered to be specific for glia and glioma cells as glutamine synthetase (GS) converts [4–^{13}C]glutamate into [4–^{13}C]glutamine. PC activity generates efflux of labeled glutamine to the extracellular compartment due to mass-balance constraints. [4–^{13}C]Glutamine is transferred to the neuronal compartment through the glutamate/glutamine cycle involved in excitatory neurotransmission, converted back to [4–^{13}C]glutamate which is then released into the extracellular space during synaptic transmission to enter again the GBM-glial compartment. Further turns of the TCA cycle will similarly label [3–^{13}C] and [2–^{13}C]glutamate and glutamine. (*b*) Metabolic fluxes quantified from compartmental modeling in healthy brains ($n = 6$) and tumor bearing brains ($n = 3$) under infusion of [1,6-^{13}C]glucose (Glc). Errors express SD derived from Monte Carlo simulations with a set of $N = 300$ artificial set of curves for Glu, Gln C4, C3 and C2. Cerebral metabolic rate of glucose ($CMR_{glc(ox)}$) is calculated as $(V^n_{TCA} + V^g_{TCA} + V_{PC})/2$. Significant correlations are indicated (*$p < 0.05$, ***$p < 0.001$, Student's *t*-test with Bonferroni's correction). [Color figure can be viewed at wileyonlinelibrary.com]

significant fraction of the cells included in the volume of interest (63–65%), the increased size of the Gln pool in injected mice suggests that GBM cells might be metabolically similar to glial cells. In previous *ex vivo* studies,[8] it was shown that GBM cells have an oxidative activity, can also metabolize other substrates than glucose and supply anaplerosis. These metabolic functions are similar to the ones of the glial compartment used in ^{13}C two-compartment modeling.[16] Therefore, the GBM cells were included in the same kinetic compartment for the analysis. Thus, Gln was entirely attributed to the glial-GBM compartment. In the analysis of the temporal evolution of metabolite concentrations measured by ^{1}H MRS, Gln mostly aligned with the primary axis in anticorrelation with NAA, Glu and GABA (Fig. 3*a*).

Therefore, Gln concentrations increased with the concomitant decrease in NAA, paralleling an augmented presence of GBM cells relative to neurons. Previously published studies in different orthotopic mouse models have been reporting discordant values for Gln variations in GBM,[30] reporting either unchanged levels[6] or decreasing Gln concentrations,[7] possibly reflecting different GBM cell densities or metabolic heterogeneities between the different models. The presence of a large Gln pool compared to normal brain, and higher ^{13}C-labeling in Gln signals in presence of significant glucose oxidation have also been reported in *ex vivo* ^{13}C MRS studies on a mouse model obtained from glioma spheres,[8] similar to our findings (Supporting Information Fig. S3 and Fig. 6). Our *in vivo* observations also support the conclusion that glioma cells are able to metabolize glucose in the mitochondria for the synthesis of Glu and Gln. Moreover, glioma cells preserve significant anaplerotic activity through pyruvate carboxylation (V_{PC}) similarly to control conditions (Fig. 6*b*).

In summary, our longitudinal ^{1}H MRS data described the infiltrative growth of human GBM cells and their metabolic characteristics, which have not yet been explored *in vivo*. The trend of a temporal shift of the changes in the metabolic profiles of WIF1 expressing xenografts to later time points, is in agreement with our previous observations of decreased migratory potential and prolonged survival mediated by attenuation of the WNT-pathway.[10] The metabolic profiles shown at late stage differ from human high grade glioma by their relatively low levels of lactate, myo-inositol and glycine. A striking observation was the presence of a substantial oxidative glucose metabolism in glioma cells, in absence of increased glycolytic rates, as revealed by ^{13}C MRS and ^{18}FDG PET. Therefore, we conclude that citric acid cycle activity, anaplerosis and synthesis of glucose-derived glutamine may be active pathways during tumor infiltration *in vivo*, which reveals an unexpected metabolic difference between glioma cells when compared to highly glycolytic cells, which have been mostly associated with necrosis and hypoxia in previous studies. This metabolic difference certainly needs to be taken into account when devising novel treatment strategies targeting the invasive front.

References

1. Lan X, Jörg DJ, Cavalli FMG, et al. Fate mapping of human glioblastoma reveals an invariant stem cell hierarchy. *Nature* 2017;549:227–32.
2. Keunen O, Taxt T, Gruner R, et al. Multimodal imaging of gliomas in the context of evolving cellular and molecular therapies. *Adv Drug Deliv Rev* 2014;76:98–115.
3. Oz G, Alger JR, Barker PB, et al. Clinical proton MR spectroscopy in central nervous system disorders. *Radiology* 2014;270:658–79.
4. Mlynarik V, Gambarota G, Frenkel H, et al. Localized short-echo-time proton MR spectroscopy with full signal-intensity acquisition. *Magn Reson Med* 2006;56:965–70.
5. Mlynarik V, Cudalbu C, Xin L, et al. ^{1}H NMR spectroscopy of rat brain *in vivo* at 14.1Tesla: improvements in quantification of the neurochemical profile. *J Magn Reson* 2008;194:163–8.
6. Hulsey KM, Mashimo T, Banerjee A, et al. ^{1}H MRS characterization of neurochemical profiles in orthotopic mouse models of human brain tumors. *NMR Biomed* 2015;28:108–15.
7. Mlynarik V, Cudalbu C, Clement V, et al. *In vivo* metabolic profiling of glioma-initiating cells using proton magnetic resonance spectroscopy at 14.1 Tesla. *NMR Biomed* 2012;25:506–13.
8. Marin-Valencia I, Yang C, Mashimo T, et al. Analysis of tumor metabolism reveals mitochondrial glucose oxidation in genetically diverse human glioblastomas in the mouse brain *in vivo*. *Cell Metab* 2012;15:827–37.
9. Maher EA, Marin-Valencia I, Bachoo RM, et al. Metabolism of [U-13 C]glucose in human brain tumors *in vivo*. *NMR Biomed* 2012;25:1234–44.
10. Vassallo I, Zinn P, Lai M, et al. WIF1 re-expression in glioblastoma inhibits migration through attenuation of non-canonical WNT signaling by downregulating the lncRNA MALAT1. *Oncogene* 2016;35:12–21.
11. Sciuscio D, Diserens AC, van Dommelen K, et al. Extent and patterns of MGMT promoter methylation in glioblastoma- and respective glioblastoma-derived spheres. *Clin Cancer Res* 2011;17:255–66.
12. Bady P, Diserens AC, Castella V, et al. DNA fingerprinting of glioma cell lines and considerations on similarity measurements. *Neuro Oncol* 2012; 14:701–11.
13. Kurscheid S, Bady P, Sciuscio D, et al. Chromosome 7 gain and DNA hypermethylation at the HOXA10 locus are associated with expression of a stem cell related HOX-signature in glioblastoma. *Genome Biol* 2015;16:16.
14. Lanz B, Rackayova V, Braissant O, et al. MRS studies of neuroenergetics and glutamate/glutamine exchange in rats: extensions to hyperammonemic models. *Anal Biochem* 2017;529:245–69.
15. Mashimo T, Pichumani K, Vemireddy V, et al. Acetate is a bioenergetic substrate for human glioblastoma and brain metastases. *Cell* 2014;159: 1603–14.
16. Lai M, Lanz B, Poitry-Yamate C, et al. *In vivo* (13)C MRS in the mouse brain at 14.1 Tesla and metabolic flux quantification under infusion of [1,6-(13)C2]glucose. *J Cereb Blood Flow Metab* 2017;1. doi:10.1177/0271678X17734101. epub ahead of print
17. Romesburg HC. Exploring, confirming, and randomization tests. *Comput Geosci* 1985;11:19–37.
18. Josse J, Husson F. Handling missing values in exploratory multivariate data analysis methods. *J Soc Fr Statistique* 2012;153:1–21.
19. R Core Team. A language and environment for statistical computing. R Foundation for Statistical Computing: Vienna, Austria, 2015. http://www.R-project.org.
20. Chessel D, Dufour AB, Thioulouse J. The ade4 package-I-one-table methods. *R News* 2004;4:5–10.
21. Tkac I, Henry PG, Andersen P, et al. Highly resolved *in vivo* 1H NMR spectroscopy of the mouse brain at 9.4 T. *Magn Reson Med* 2004;52:478–84.
22. Lambiv WL, Vassallo I, Delorenzi M, et al. The Wnt inhibitory factor 1 (WIF1) is targeted in glioblastoma and has a tumor suppressing function potentially by induction of senescence. *Neuro Oncol* 2011;13:736–47.
23. Alger JR, Frank JA, Bizzi A, et al. Metabolism of human gliomas: assessment with H-1 MR spectroscopy and F-18 fluorodeoxyglucose PET. *Radiology* 1990;177:633–41.
24. Lupo JM, Cha S, Chang SM, et al. Analysis of metabolic indices in regions of abnormal perfusion in patients with high-grade glioma. *AJNR Am J Neuroradiol* 2007;28:1455–61.
25. Agnihotri S, Zadeh G. Metabolic reprogramming in glioblastoma: the influence of cancer metabolism on epigenetics and unanswered questions. *Neuro Oncol* 2016;18:160–72.
26. Kathagen-Buhmann A, Schulte A, Weller J, et al. Glycolysis and the pentose phosphate pathway are differentially associated with the dichotomous regulation of glioblastoma cell migration versus proliferation. *NEUONC* 2016;18:1219–29.
27. Talasila KM, Rosland GV, Hagland HR, et al. The angiogenic switch leads to a metabolic shift in human glioblastoma. *Neuro Oncol* 2017;19:383–93.
28. Bougnaud S, Golebiewska A, Oudin A, etet al. Molecular crosstalk between tumour and brain parenchyma instructs histopathological features in glioblastoma. *Oncotarget* 2016;22:31955–71.
29. Terpstra M, Gruetter R, High WB, et al. Lactate turnover in rat glioma measured by *in vivo* nuclear magnetic resonance spectroscopy. *Cancer Res* 1998;58:5083–8.
30. Doblas S, He T, Saunders D, et al. *In vivo* characterization of several rodent glioma models by 1H MRS. *NMR Biomed* 2012;25:685–94.

THE DIFFERENCE OF BREAKTHROUGH DISCOVERIES ON YOUR TERMS

WITH AN APPROACHABLE, AFFORDABLE, AUTOMATED 4-WAY CELL SORTING SOLUTION IN YOUR LAB. Cell sorting may be complex but it doesn't need to feel complicated or out of reach. With intuitive software that requires minimal training, the BD FACSMelody™ Cell Sorter enables deep scientific insights with reliable results, cost savings and workflow efficiencies. Discover how better instrumentation can free up your time so you can focus your expertise where it matters most. **Discover the new BD.**

Learn how you can advance your research >

BD